Simulation of the quantum dynamics of indistinguishable bosons with the method of coupled coherent states

James A. Green* and Dmitrii V. Shalashilin†
School of Chemistry, University of Leeds, Leeds LS2 9JT, United Kingdom

(Received 7 January 2019; published 10 July 2019)

Computer simulations of many-body quantum dynamics of indistinguishable particles is a challenging task for computational physics. In this paper we demonstrate that the method of coupled coherent states (CCS) developed previously for multidimensional quantum dynamics of distinguishable particles can be used to study indistinguishable bosons in the second-quantization formalism. To prove its validity, the technique termed here coupled coherent states for indistinguishable bosons (CCSB) is tested on two model problems. The first is a system-bath problem consisting of a tunneling mode coupled to a harmonic bath, previously studied by CCS and other methods in distinguishable representation in 20 dimensions. The harmonic bath is comprised of identical oscillators, and may be second quantized for use with CCSB, so that this problem may be thought of as a bosonic bath with an impurity. The cross-correlation function for the dynamics of the system and Fourier transform spectrum compare extremely well with a benchmark calculation, which none of the prior methods of studying the problem achieved. The second model problem involves 100 bosons in a shifted harmonic trap. Breathing oscillations in the one-body density are calculated and shown to compare favorably to a multiconfigurational time-dependent Hartree for bosons calculation, demonstrating the applicability of the method as a new formally exact way to study the quantum dynamics of Bose-Einstein condensates.

DOI: 10.1103/PhysRevA.100.013607

I. INTRODUCTION

In the past two decades there has been significant interest in systems of indistinguishable bosons due to experimentally produced Bose-Einstein condensates of ultracold alkali metal atoms [1–3]. These condensates, first posited by the eponymous Bose and Einstein in 1924–1925, have permitted macroscopic observations of quantum phenomena and led to a wealth of experimental research in areas such as atomic interferometry [4], bosonic Josephson junctions [5,6], quantum vortices [7,8], and the generation of solitons [9,10].

From the theoretician's point of view, the Gross-Pitaevskii equation (GPE) [11,12] has been the predominant method used to study Bose-Einstein condensates; see, for example, Refs. [13–18] and the review articles [19,20]. However the GPE is a mean-field theory and as such cannot describe many-body effects in condensates. It also assumes that all bosons occupy a single state at all times, which is not the case during fragmentation. In recent years, the multiconfigurational time-dependent Hartree method for bosons (MCTDHB) [21,22] has been used to treat indistinguishable bosons from the standpoint of exact quantum mechanics [23–33]. A multilayer version of MCTDHB has also been developed (ML-MCTDHB) [34,35] that exploits the multilayer structure to study mixed bosonic systems (for example, impurities in Bose-Einstein condensates [36–40], binary mixtures of Bose-Einstein condensates [41], and solitons [40,42–44]) and bosonic systems where different degrees of freedom may be separated (for example different spatial locations when bosons are residing in optical lattices [45–52]).

Before being used to treat indistinguishable bosons, standard MCTDH [53] and ML-MCTDH [54,55] have been well established theories for treating distinguishable particles. They are able to solve the time-dependent Schrödinger equation (TDSE) exactly for multiple degrees of freedom, albeit with basis sets that grow exponentially with increased dimensionality. Our own coupled coherent states (CCS) method has also demonstrated its propensity at solving the TDSE for distinguishable particles, with basis sets that scale more favorably with dimensionality [56,57]. This is achieved by using randomly sampled trajectory guided coherent states as basis functions, although the trade-off for this favorable scaling is that random noise and slow convergence may be present. Noise can cause a decay in auto- or cross-correlation functions and may be reduced by increasing the number of configurations, or applying a filter diagonalization technique to extract frequencies [58]. Importance sampling of coherent state basis set initial conditions is also key to the accuracy and efficiency of the CCS approach [59].

In this present work we extend the CCS method to looking at indistinguishable bosons in the second-quantization representation, and dub the method coupled coherent states for indistinguishable bosons (CCSB). Due to the use of coherent states in CCSB and their relation to the creation and annihilation operators of second quantization, together with the fact that systems with a large number of particles tend towards classical behavior and the basis in CCSB is guided by classical-like trajectories, suggest that the method

*Present address: Consiglio Nazionale delle Ricerche, Istituto di Biostrutture e Bioimmagini (CNR-IBB), via Mezzocannone 16, 80134, Napoli, Italy; j.a.green1@leeds.ac.uk
†d.shalashilin@leeds.ac.uk

will be particularly suited to such systems. Indeed, recent semiclassical coherent state work with the Herman-Kluk method on indistinguishable bosons demonstrates this hypothesis [60,61]. CCSB is fully quantum however, as with standard CCS, and it has previously been shown that a local quadratic approximation of the Hamiltonian into the CCS equations yields the coherent state matrix of the Herman-Kluk propagator [62]. We anticipate that the CCSB method will provide a description of many-body dynamics over and above the mean-field Gross-Pitaevskii approach. Furthermore, as CCS has previously shown to be able to provide a similar numerical picture to MCTDH with lower computational scaling with dimensionality [63], we anticipate that CCSB may be able to do the same with respect to MCTDHB.

To illustrate the suitability of CCSB to problems involving indistinguishable bosons, we apply the method to two model problems. The first model problem consists of a bosonic bath with an impurity, demonstrating that the method is capable of studying multicomponent bosonic systems and opening up the possibility of studying multi-atomic Bose-Einstein condensates [64], spinor Bose-Einstein condensates [65], dark-bright solitons [66], and Bose-polarons [67]. The second model problem consists of a collection of indistinguishable bosons in a harmonic trap, demonstrating the propensity of the method to study systems of bosons in optical lattices [68]; for example, with the Bose-Hubbard model [60,61,69], and the possibility to study bosons in a single well that is deformed into a double well, such as that in Ref. [22], and observed in experimental bosonic Josephson junctions [70,71].

II. NUMERICAL DETAILS

The CCSB method relies on the machinery of the CCS method, which has been derived and presented previously when treating distinguishable particles [56,57]. A description of the CCS method will be presented below, before a discussion on how the method is modified to treat indistinguishable bosons in the second-quantization representation in CCSB.

A. Coupled coherent states working equations

In the CCS method, the wave function is represented as a basis set of trajectory guided coherent states, $|z\rangle$. The coordinate representation of a coherent state is given by

$$\langle x|z\rangle = \left(\frac{\gamma}{\pi}\right)^{1/4} \exp\left[-\frac{\gamma}{2}(x-q)^2 + \frac{i}{\hbar}p(x-q) + \frac{ipq}{2\hbar}\right], \tag{1}$$

where q and p are the position and momentum centers of the coherent state, γ is the width parameter of the coherent state, given by $\gamma = m\omega/\hbar$, with m mass and ω frequency. In atomic units (which are used throughout the paper) $m = \omega = \hbar = 1$, thus $\gamma = 1$. Coherent states are eigenstates of the creation and annihilation operators respectively

$$\langle z|\,\hat{a}^\dagger = \langle z|\,z^*, \tag{2a}$$

$$\hat{a}\,|z\rangle = z\,|z\rangle\,, \tag{2b}$$

where the creation and annihilation operators are given by

$$\hat{a}^\dagger = \frac{1}{\sqrt{2}}(\hat{q} - i\hat{p}), \tag{3a}$$

$$\hat{a} = \frac{1}{\sqrt{2}}(\hat{q} + i\hat{p}). \tag{3b}$$

The eigenvalues of Eqs. (2a) and (2b), z^* and z, can be used to label a coherent state, and from Eqs. (3a) and (3b) it can be seen they are given by

$$z^* = \frac{1}{\sqrt{2}}(q - ip), \tag{4a}$$

$$z = \frac{1}{\sqrt{2}}(q + ip). \tag{4b}$$

An important consequence of the above is that one may write a Hamiltonian in terms of creation and annihilation operators rather than position and momentum operators. A normal-ordered Hamiltonian may then be obtained when the creation operators precede the annihilation ones:

$$\hat{H}(\hat{q},\hat{p}) = \hat{H}(\hat{a},\hat{a}^\dagger) = H_{\rm ord}(\hat{a}^\dagger,\hat{a}). \tag{5}$$

From this, matrix elements of the Hamiltonian are simple to calculate in a coherent state basis:

$$\langle z'|H_{\rm ord}(\hat{a}^\dagger,\hat{a})|z\rangle = \langle z'|z\rangle\, H_{\rm ord}(z'^*, z), \tag{6}$$

where the overlap $\langle z'|z\rangle$ is given by

$$\langle z'|z\rangle = \exp\left(z'^* z - \frac{z'^* z'}{2} - \frac{z^* z}{2}\right). \tag{7}$$

The wave function ansatz in CCS is given by

$$|\Psi(t)\rangle = \sum_{k=1}^{K} D_k(t) e^{iS_k(t)}\,|z_k(t)\rangle\,, \tag{8}$$

where the sum is over K configurations, D_k is a time-dependent amplitude and S_k is the classical action. The classical action in coherent-state notation is given by

$$S_k = \int \left[\frac{i}{2}(z_k^*\dot{z}_k - \dot{z}_k^* z_k) - H_{\rm ord}(z_k^*, z_k)\right]dt. \tag{9}$$

The wave function is propagated via the time dependence of the coherent-state basis vectors, amplitudes, and action. The coherent states are guided by classical trajectories and evolve according to Hamilton's equation:

$$\dot{z}_k = -i\frac{\partial H_{\rm ord}(z_k^*, z_k)}{\partial z_k^*}. \tag{10}$$

The time-dependence of the amplitudes may be found via substitution of Eq. (8) into the time-dependent Schrödinger equation and closing with a coherent-state basis bra:

$$\sum_{l=1}^{K} \langle z_k|z_l\rangle\, e^{iS_l}\frac{dD_l}{dt} = -i\sum_{l=1}^{K}\langle z_k|z_l\rangle\, e^{iS_l} D_l \delta^2 H'_{\rm ord}(z_k^*, z_l), \tag{11}$$

where the $\delta^2 H'_{\rm ord}(z_k^*, z_l)$ term is

$$\delta^2 H'_{\rm ord}(z_k^*, z_l) = H_{\rm ord}(z_k^*, z_l) - H_{\rm ord}(z_l^*, z_l) - i\dot{z}_l(z_k^* - z_l^*). \tag{12}$$

Finally, the time dependence of the classical action is straightforwardly calculated from Eq. (9).

B. Second quantization and coupled coherent states for indistinguishable bosons

CCS works for Hamiltonians that can be expressed via creation and annihilation operators in the normal-ordered form as illustrated in Eq. (6). In second quantization, the Hamiltonian of a system of bosons also appears in a normal ordered form, therefore no modifications of the CCS working equations are required for treating indistinguishable bosons with CCSB. The only difference is that the coherent-state basis functions are used to represent particle number occupations of quantum states in the second-quantization formalism, as opposed to individual particles in the distinguishable first-quantization representation.

In the second-quantization representation, multiparticle states are described in terms of an occupation number $n^{(\alpha)}$ that describes the number of particles belonging to a particular quantum state $|\alpha\rangle$. A Fock state describes the set of occupation number states:

$$|\mathbf{n}\rangle = \prod_{\alpha=0}^{\Omega} |n^{(\alpha)}\rangle = |n^{(0)},\ n^{(1)}, \ldots, n^{(\Omega)}\rangle\,, \tag{13}$$

and may be generated by successive application of creation operators on the vacuum state $|0\rangle$:

$$|n^{(0)},\ n^{(1)}, \ldots, n^{(\Omega)}\rangle = \frac{(\hat{a}^{(0)\dagger})^{n^{(0)}}}{\sqrt{n^{(0)}!}} \frac{(\hat{a}^{(1)\dagger})^{n^{(1)}}}{\sqrt{n^{(1)}!}} \cdots \frac{(\hat{a}^{(\Omega)\dagger})^{n^{(\Omega)}}}{\sqrt{n^{(\Omega)}!}} |0^{(0)},\ 0^{(1)}, \ldots, 0^{(\Omega)}\rangle\,. \tag{14}$$

In CCSB, the multidimensional version of the CCS wavefunction representation is used as a basis set expansion for Fock states:

$$|\mathbf{n}\rangle = \sum_{k=1}^{K} D_k(t) e^{iS_k(t)}\, |\mathbf{z}_k(t)\rangle\,, \tag{15}$$

which is exactly analogous to Eq. (8). The only difference is the multidimensional coherent state $|\mathbf{z}_k\rangle$ is a product of coherent states that describe occupations of each quantum state $|\alpha\rangle$:

$$|\mathbf{z}_k\rangle = \prod_{\alpha=0}^{\Omega} |z^{(\alpha)}\rangle\,. \tag{16}$$

Therefore any wave function in the basis of Fock states can be equivalently represented in the basis of coherent states. The Hamiltonian of a system of indistinguishable bosons can be second quantized and presented in terms of one-body $\hat{h}(\mathbf{Q})$, two-body $\hat{W}(\mathbf{Q}, \mathbf{Q}')$, and creation and annihilation operators as

$$\hat{H} = \sum_{\alpha,\beta} \langle\alpha|\hat{h}|\beta\rangle\, \hat{a}^{(\alpha)\dagger}\hat{a}^{(\beta)} + \frac{1}{2} \sum_{\alpha,\beta,\gamma,\zeta} \langle\alpha,\beta|\hat{W}|\gamma,\zeta\rangle\, \hat{a}^{(\alpha)\dagger}\hat{a}^{(\beta)\dagger}\hat{a}^{(\zeta)}\hat{a}^{(\gamma)}, \tag{17}$$

where $|\alpha\rangle$, $|\beta\rangle$, $|\gamma\rangle$, and $|\zeta\rangle$ are quantum states. This conveniently gives a second-quantized Hamiltonian in normal-ordered form, which is required by CCSB. In the following sections CCSB is applied to two model problems to illustrate its ability to study fully quantum bosonic problems and compare with numerically exact results.

III. APPLICATION 1: DOUBLE-WELL TUNNELLING PROBLEM

The first application of CCSB is to an M-dimensional model Hamiltonian that consists of an $(M-1)$-dimensional harmonic bath, coupled to a one-dimensional tunneling mode governed by an asymmetric double-well potential. This a system-bath problem, which may also be thought of as a bosonic bath with an impurity, previously studied in distinguishable representation with linear coupling of the bath to the system by matching pursuit split-operator Fourier transform (MP/SOFT) [72], standard CCS [73], a trajectory guided configuration-interaction (CI) expansion of the wave function [74], an adaptive trajectory guided (aTG) scheme [75], Gaussian process regression (GPR) [76], and a basis expansion leaping multiconfiguration Gaussian (BEL MCG) method [77]. It has also been studied with quadratic coupling of the bath to the system by MP/SOFT [72], standard CCS [73], trajectory guided CI [74], aTG [75], and a two-layer version of CCS (2L-CCS) [78]. A benchmark calculation for the quadratic-coupling case has also been proposed in recent work [79] by using a relatively simple wave-function expansion in terms of particle in a box wave functions for the tunneling mode, and harmonic-oscillator wave functions for the harmonic bath. The size of the calculation in Ref. [79] was greatly reduced by exploiting the indistinguishability of the bath configurations, and a well-converged result was achieved, prompting the idea of CCSB. The quadratic coupling case is the one we consider in this application.

The Hamiltonian is given in distinguishable representation by

$$\hat{H} = \frac{\hat{p}^{(1)^2}}{2} - \frac{\hat{q}^{(1)^2}}{2} + \frac{\hat{q}^{(1)^4}}{16\eta} + \frac{\hat{\mathbf{P}}^2}{2} + \frac{(1+\lambda\hat{q}^{(1)})\hat{\mathbf{Q}}^2}{2}, \tag{18}$$

where $(\hat{q}^{(1)}, \hat{p}^{(1)})$ are the position and momentum operators of the one-dimensional system tunneling mode, and $(\hat{\mathbf{Q}}, \hat{\mathbf{P}})$ are the position and momentum operators of the $(M-1)$-dimensional harmonic bath modes, with $\hat{\mathbf{Q}} = \sum_{m=2}^{M} \hat{q}^{(m)}$ and $\hat{\mathbf{P}} = \sum_{m=2}^{M} \hat{p}^{(m)}$. The coupling between system and bath is given by the constant λ, while η determines the well depth.

In previous work [72–75,78,79], the parameters $\lambda = 0.1$ and $\eta = 1.3544$ have been used in a 20-dimensional ($M = 20$) problem, which we also consider. The initial wave function $|\Psi(0)\rangle$ is a multidimensional Gaussian wave packet, with initial position and momentum centers for the tunneling mode $\hat{q}^{(1)}(0) = -2.5$ and $\hat{p}^{(1)}(0) = 0.0$, and for the bath modes $\hat{q}^{(m)}(0) = 0.0$ and $\hat{p}^{(m)}(0) = 0.0\ \forall\ m$.

As the bath oscillators have the same initial conditions and the same frequency, they can be thought of as indistinguishable, and the bath part of the Hamiltonian may be second quantized for use with CCSB. Because the tunneling mode is not part of this indistinguishable system, the portion of the

Hamiltonian that describes it will not be second quantized. However, this will not pose a problem as the dynamical equations are identical for CCS and CCSB, the only subtlety is the interpretation of the coherent-state basis vectors $|\mathbf{z}\rangle$ as will be discussed below. Using the definition of a second-quantized Hamiltonian in Eq. (17), and the definition of coherent states as eigenstates of the creation and annihilation operators, Eq. (18) may be written in normal-ordered form as $H_{\rm ord}(\hat{a}^\dagger, \hat{a})$, for which the coherent-state matrix element $\langle \mathbf{z}_k|H_{\rm ord}(\hat{a}^\dagger, \hat{a})|\mathbf{z}_l\rangle = \langle \mathbf{z}_k|\mathbf{z}_l\rangle\, H_{\rm ord}(\mathbf{z}_k^*, \mathbf{z}_l)$, where

$$\begin{aligned} H_{\rm ord}(\mathbf{z}_k^*, \mathbf{z}_l) = &-\frac{1}{2}\left(z_k^{(m=1)*^2} + z_l^{(m=1)^2}\right) + \frac{1}{64\eta}\left(z_k^{(m=1)*^4}\right. \\ &+ z_l^{(m=1)^4} + 4z_k^{(m=1)*^3} z_l^{(m=1)} + 4z_k^{(m=1)*} z_l^{(m=1)^3} \\ &+ 6z_k^{(m=1)*^2} z_l^{(m=1)^2} + 12 z_k^{(m=1)*} z_l^{(m=1)} + 6 z_k^{(m=1)*^2} \\ &\left. + 6z_l^{(m=1)^2} + 3\right) + \sum_{\alpha=0}^{\Omega} z_k^{(2\alpha)*} z_l^{(2\alpha)} \epsilon^{(2\alpha)} \\ &+ \frac{\lambda}{2} \sum_{\alpha,\beta=0}^{\Omega} z_k^{(2\alpha)*} z_l^{(2\beta)} Q^{(2\alpha,2\beta)^2} \left(z_k^{(m=1)*} + z_l^{(m=1)}\right). \end{aligned} \tag{19}$$

The quantum states $|\alpha\rangle$ and $|\beta\rangle$ in Eq. (19) are those of the harmonic oscillator with α and β numbers of quanta, $\epsilon^{(\alpha)}$ is the eigenvalue for $|\alpha\rangle$, and the position and momentum operators of the tunneling mode have explicitly been labeled with $(m = 1)$ to distinguish them from the α labeling scheme of the second-quantized bath modes. A full derivation of this, alongside evaluation of the $Q^{(2\alpha,2\beta)^2}$ matrix element is shown in Appendix A. Note that only even harmonic-oscillator levels are required due to all bath modes initially residing in the ground level, as previously assumed [79], and the bath having quadratic coupling to the system meaning only even harmonic-oscillator levels will be occupied.

The multidimensional coherent-state basis vector $|\mathbf{z}\rangle$ is represented as

$$|\mathbf{z}\rangle = |z^{(m=1)}\rangle \times \prod_{\alpha=0}^{\Omega} |z^{(2\alpha)}\rangle\,, \tag{20}$$

where $|z^{(m=1)}\rangle$ is a basis function for the tunneling mode and $|z^{(2\alpha)}\rangle$ is a basis function for the second-quantized bath modes. The determination of initial conditions for these coherent-state basis functions, as well as the values of the initial amplitudes is shown in the following section.

A. Initial conditions for Application 1

The initial coherent-state basis functions for the tunneling mode are sampled from a Gaussian distribution centered around the initial tunneling mode coordinates and momenta, as in previous works [73,78]:

$$f(z^{(m=1)}) \propto \exp(-\sigma^{(m=1)}|z^{(m=1)} - z^{(m=1)}(0)|^2), \tag{21}$$

where $\sigma^{(m=1)}$ is a parameter governing the width of the distribution.

Sampling the initial coherent states for the bath can be performed by obtaining a probability distribution from the square of the coherent-state representation of the initial bath Fock state. The initial bath Fock state is equal to

$$\begin{aligned} |\mathbf{n}\rangle &= \prod_{\alpha=0}^{\Omega} |n^{(2\alpha)}\rangle \\ &= |n^{(2\alpha=0)}, n^{(2\alpha=2)}, \ldots, n^{(2\alpha=2\Omega)}\rangle \\ &= |(M-1), 0, \ldots, 0\rangle\,, \end{aligned} \tag{22}$$

where there are $M - 1$ bath oscillators all in the ground harmonic-oscillator state. Using the representation of a coherent state in a basis of Fock states,

$$|z\rangle = e^{-\frac{|z|^2}{2}} \sum_{n^{(\alpha)}} \frac{z^{n^{(\alpha)}}}{\sqrt{(n^{(\alpha)}!)}}\, |n^{(\alpha)}\rangle\,, \tag{23}$$

the following may be obtained:

$$|\,\langle z^{(2\alpha)}|n^{(2\alpha)}\rangle\,|^2 = \frac{e^{-|z^{(2\alpha)}|^2}(|z^{(2\alpha)}|^2)^{n^{(2\alpha)}}}{\pi\, n^{(2\alpha)}!}, \tag{24}$$

where the value of π has appeared to enforce normalization. This resembles a Poissonian distribution; however, $|z^{(2\alpha)}|^2$ is continuous so a gamma distribution is used instead:

$$f(|z^{(2\alpha)}|^2) \propto \frac{(|z^{(2\alpha)}|^2)^{n^{(2\alpha)}} e^{\frac{-|z^{(2\alpha)}|^2}{\sigma^{(2\alpha)}}}}{\Gamma(n^{(2\alpha)}+1)(\sigma^{(2\alpha)})^{n^{(2\alpha)}+1}}, \tag{25}$$

where $\sigma^{(2\alpha)}$ is a compression parameter controlling the width of the distribution, and Γ is the gamma function that is calculated by using $n^{(2\alpha)} + 1$ because $\Gamma(n) = (n-1)!$.

The gamma distribution will be centered around $\sigma^{(2\alpha)} n^{(2\alpha)}$; however, $|\,\langle z^{(2\alpha)}|n^{(2\alpha)}\rangle\,|^2$ should be centered around $|z^{(2\alpha)}|^2 = n^{(2\alpha)}$ because its maximum is found by

$$\begin{aligned} \frac{d|\,\langle z^{(2\alpha)}|n^{(2\alpha)}\rangle\,|^2}{d|z^{(2\alpha)}|^2} = \frac{1}{\pi\, n^{(2\alpha)}!}\big[&- e^{-|z^{(2\alpha)}|^2}(|z^{(2\alpha)}|^2)^{n^{(2\alpha)}} \\ &+ n^{(2\alpha)} e^{-|z^{(2\alpha)}|^2}(|z^{(2\alpha)}|^2)^{n^{(2\alpha)}-1}\big] = 0. \end{aligned} \tag{26}$$

Fortunately, this is not an issue, because when $n^{(2\alpha)} = 0$ for states $2\alpha > 0$, the distribution will be centered around 0 irrespective of the compression parameter, and for $n^{(2\alpha=0)} = M - 1$ a compression parameter of $\sigma^{(2\alpha=0)} = 1.0$ is used. Because we are not constrained by a choice of compression parameter $\sigma^{(2\alpha>0)}$ for the states $2\alpha > 0$, we are free to alter it to influence the accuracy of the calculation, and the final result presented in the following section uses $\sigma^{(2\alpha>0)} = 100$. The affect of altering this parameter is discussed in Sec. III C.

The initial amplitudes are calculated by projection of the initial basis onto the initial wave function with the action set to zero:

$$\langle \mathbf{z}_k(0)|\Psi(0)\rangle = \sum_{l=1}^{K} D_l(0)\, \langle \mathbf{z}_k(0)|\mathbf{z}_l(0)\rangle\,. \tag{27}$$

The overlap of the initial coherent-state basis with the initial wave function can be decomposed to

$$\langle \mathbf{z}_k(0)|\Psi(0)\rangle = \langle z_k^{(m=1)}(0)|\Psi^{(m=1)}(0)\rangle \left\langle \prod_{\alpha=0}^{\Omega} z_k^{(2\alpha)}(0)|\mathbf{n}\right\rangle. \quad (28)$$

The coherent-state overlap with initial tunneling mode wave function $\langle z_k^{(m=1)}(0)|\Psi^{(m=1)}(0)\rangle$ can be calculated via a Gaussian overlap, Eq. (7), by using the initial positions and momenta for the tunneling mode $\hat{q}^{(m=1)}(0) = -2.5$ and $\hat{p}^{(m=1)}(0) = 0.0$. The coherent-state overlap with the initial bath Fock state can be calculated by once more using the coherent-state representation in a basis of Fock states, Eq. (23),

$$\left\langle \prod_{\alpha=0}^{\Omega} z_k^{(2\alpha)}(0)|\mathbf{n}\right\rangle = \left[\prod_{\alpha=0}^{\Omega} e^{-\frac{|z_k^{(2\alpha)}(0)|^2}{2}}\right] \frac{\left(z_k^{(2\alpha=0)*}(0)\right)^{M-1}}{\sqrt{(M-1)!}}. \quad (29)$$

B. Results and comparison to other methods

The quantity of interest used to assess the performance of CCSB and compare it to previous methods of studying the problem [72–75,78,79] is the cross-correlation function (CCF). This is the overlap between the wave function at time t and the mirror image of the initial wave packet, $|\bar{\Psi}(0)\rangle$, i.e., $\langle\bar{\Psi}(0)|\Psi(t)\rangle$. The mirror image of the initial state has coordinates for the tunneling mode of $\bar{q}^{(1)}(0) = +2.5$ and $\bar{p}^{(1)}(0) = 0.0$, with bath modes in the ground harmonic level. It is located in the upper well of the asymmetric double-well tunneling potential, therefore nonzero values of the CCF are indicative of tunneling. The spectrum of the CCF is also presented via a Fourier transform (FT) of the real part of the CCF.

The results of the CCSB calculation compared with previous methods of studying the twenty-dimensional (20D), $\lambda = 0.1$ case [72–75,78,79] is shown in Fig. 1 with the absolute values of the CCFs in Fig. 1(i), and FT spectra in Fig. 1(ii). As can be seen from these two figures, the CCSB results compare extremely favorably to the benchmark calculation, with much closer agreement than prior methods. Previously, the trajectory guided CI expansion was the closest result to the benchmark, due to its basis set expansion of time-independent basis functions used to represent excited-state configurations being similar to the benchmark approach. However, the CCF still differed from the benchmark, with noticeable differences occurring after 25 a.u., possibly due to approximations used in sampling the potential-energy surface, despite the FT obtaining splitting of the higher-energy peaks that no prior method managed. For this present CCSB calculation, there is no significant degradation of the calculation at $t > 25$ a.u. as with the other methods, and the splitting of the high-energy peaks is very well reproduced. As was alluded to in Ref. [78], for this Hamiltonian a detailed description of the bath is required for accurate propagation, which is achieved in CCSB by taking account of the symmetry of the Hamiltonian.

The CCSB calculation uses $K = 4000$ configurations and $\Omega = 5$ even harmonic-oscillator levels in the bath basis. The dimensionality of this problem has therefore been reduced from 20 to 6. The influence on the CCSB calculation of altering these parameters, as well as the compression parameter chosen of $\sigma^{(2\alpha>0)} = 100$ is shown in the following section.

C. Numerical accuracy and convergence

By using an approach first presented in Ref. [78] to illustrate the accuracy and convergence of a method studying Application 1 with respect to the benchmark calculation, we define an error parameter χ as

$$\chi = \int |\mathrm{Abs}(\langle\bar{\Psi}(0)|\Psi(t)\rangle)_{\mathrm{bench}} - \mathrm{Abs}(\langle\bar{\Psi}(0)|\Psi(t)\rangle)_{\mathrm{CCSB}}|dt, \quad (30)$$

which indicates the cumulative error of the absolute value of the cross-correlation function of the CCSB method compared with the benchmark. This is shown in Fig. 2(i), for different values of $\sigma^{(2\alpha>0)}$, K and Ω, in Figs. 2(i)(a)–2(i)(c).

As with CCS, the CCSB method does not conserve the norm $\langle\Psi(t)|\Psi(t)\rangle$ by default due to the use of a basis consisting of a superposition of coherent states [57]. However, this can be a useful property because the extent of norm conservation can be used to determine the accuracy and reliability of a propagation. Another important quantity for CCSB to conserve is the total particle number

$$\begin{aligned} N &= \langle\Psi(t)|\sum_{\alpha=0}^{\Omega}\hat{a}^{(\alpha)\dagger}\hat{a}^{(\alpha)}|\Psi(t)\rangle \\ &= \sum_{k,l=1}^{K}\sum_{\alpha=0}^{\Omega} D_k^* D_l e^{i(S_l-S_k)}\langle\mathbf{z}_k|\mathbf{z}_l\rangle\, z_k^{(\alpha)*} z_l^{(\alpha)}, \end{aligned} \quad (31)$$

which for Application 1 amounts to the number of oscillators in the bath, $N = (M-1) = 19$. Plots of the norm and particle number conservation for different values of $\sigma^{(2\alpha>0)}$, K, and Ω [as in Fig. 2(i)], are shown in Fig. 2(ii), with the value of the norm given by the dashed-dotted lines without circles and the particle number by the dashed-dotted lines with circles. It can be seen that the values of the norm and particle number follow each other closely for all calculations, and we will discuss the specific cases in the following.

First, considering Figs. 2(i)(a) and 2(ii)(a), both K and Ω are held fixed while $\sigma^{(2\alpha>0)}$ is varied. It can be seen that the quality of the calculation with respect to the error term χ and the conservation of the norm and particle number improve with increasing $\sigma^{(2\alpha>0)}$. A further increase of $\sigma^{(2\alpha>0)}$ results in a numerically unstable propagation, because the value of the norm and particle number explodes as the basis is overcompressed. This suggests that appropriate choice of $\sigma^{(2\alpha>0)}$ is necessary for the initial sampling of the coherent states, because a value that is too small leads to errors due to the coherent states spreading too quickly, while a value that is too large leads to numerical instability.

Second, considering Figs. 2(i)(b) and 2(ii)(b), the value of K is varied while Ω is held constant. The value of $\sigma^{(2\alpha>0)}$ was chosen based on the criteria presented in the previous paragraph, with larger values of $\sigma^{(2\alpha>0)}$ for smaller values of K. This phenomenon has been noted in previous studies with CCS, where larger compression parameters are necessary for basis sets with fewer configurations; see Ref. [59] for further details. The error χ decreases with increasing K, as Monte Carlo noise causing decay of the cross-correlation

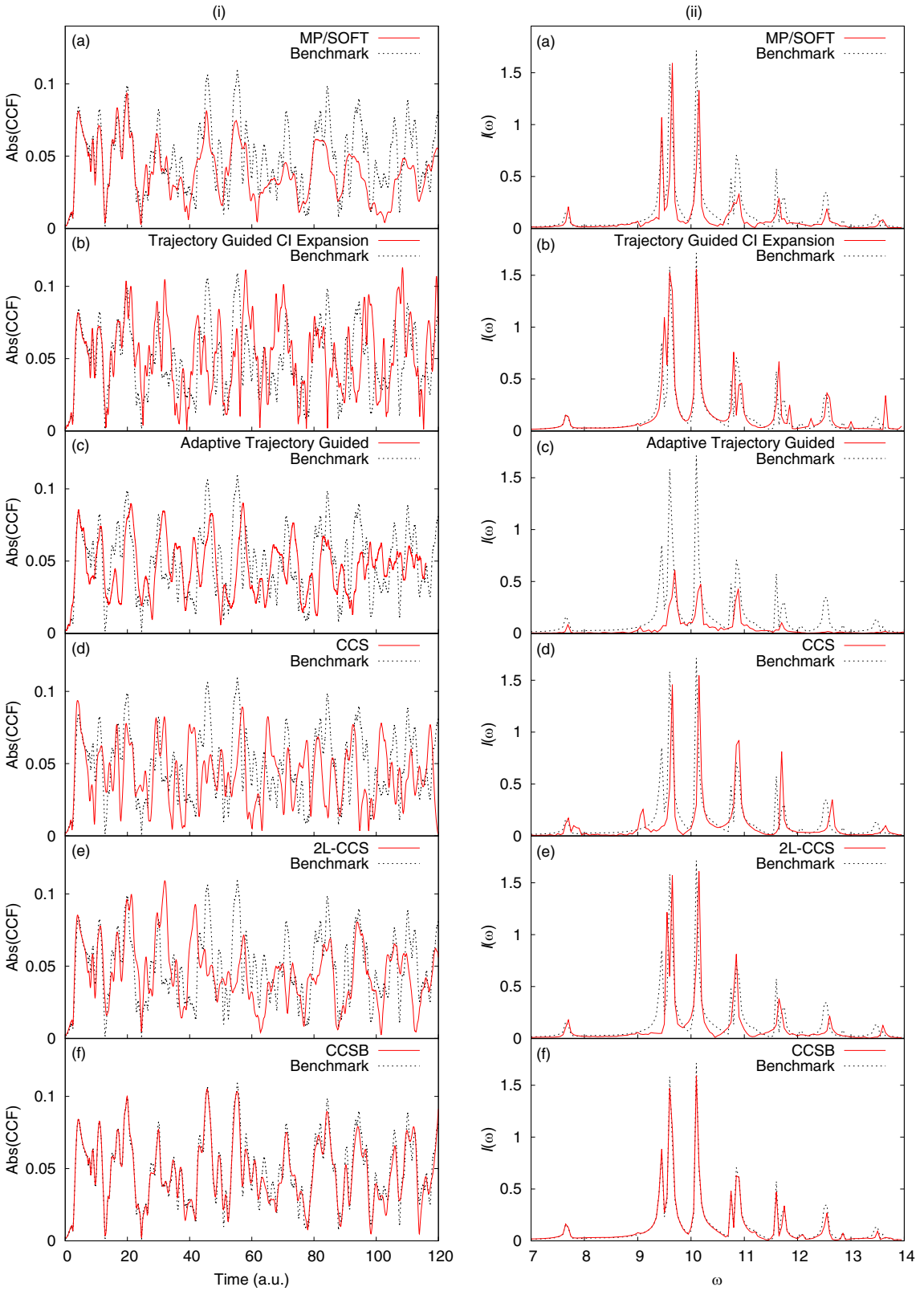

FIG. 1. Comparison of (i) absolute values of the cross-correlation functions and (ii) Fourier transforms of the real part of the cross-correlation functions for different methods (red, solid) of studying Eq. (18) with $M = 20$. $\lambda = 0.1$ parameters relative to the benchmark [79] (black, dotted): (a) MP/SOFT [72], (b) Trajectory Guided CI Expansion [74], (c) aTG [75], (d) CCS [73], (e) 2L-CCS [78], (f) CCSB (present work).

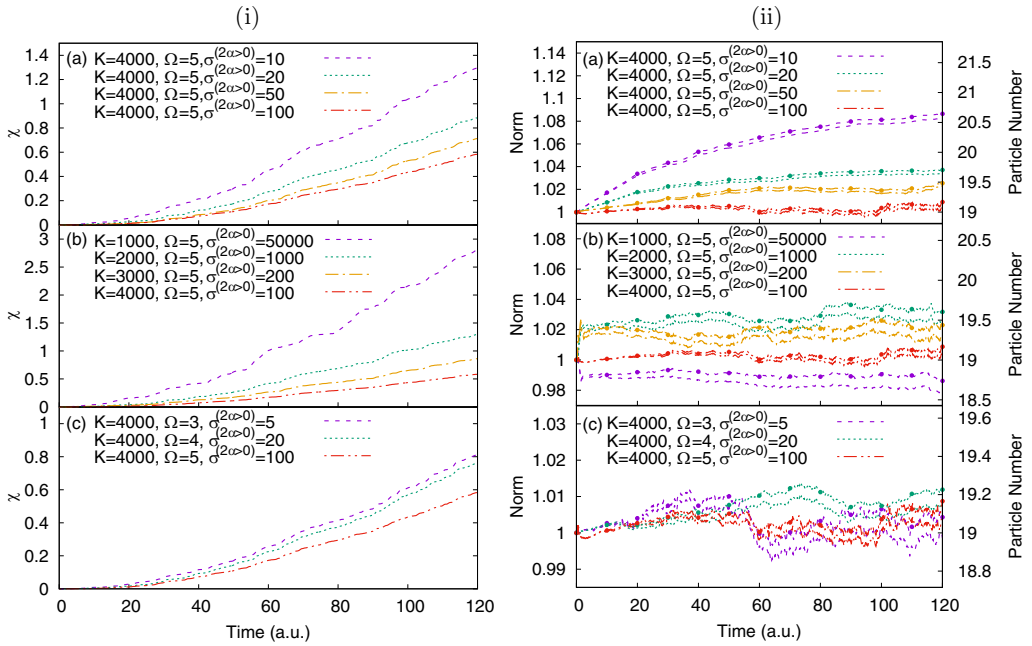

FIG. 2. (i) Cumulative error χ [defined in Eq. (30)] of the CCSB method with respect to the benchmark [79] for different values of (a) compression parameter for coherent-state sampling of the bath basis levels with zero initial occupation $\sigma^{(2\alpha>0)}$, (b) configurations K, and (c) even harmonic-oscillator levels in bath basis Ω. (ii) Norm (dashed-dotted lines without circles) and particle number (dashed-dotted lines with circles) of CCSB calculations with different values of (a) $\sigma^{(2\alpha>0)}$, (b) K, and (c) Ω. Note that in panels (b) and (c) for both columns (i) and (ii) the value of $\sigma^{(2\alpha>0)}$ changes as well as K and Ω. This is addressed in the text.

function decreases with increasing number of configurations. However, χ does not remain at 0 for the duration of the calculation, and the $K = 4000$ propagation is only equivalent to the $K = 3000$ calculation for the first 30 a.u. This indicates the slow convergence of the method as mentioned in the introduction. However, we can regard the accuracy of the $K = 4000$ calculation as sufficient for this application as we are able to obtain an accurate FT spectrum with correct frequencies, alongside the good conservation of norm and particle number compared with the other calculations with fewer configurations.

Finally, considering Figs. 2(i)(c) and 2(ii)(c), the value of Ω is varied while K is held constant. The value of $\sigma^{(2\alpha>0)}$ was again chosen based on the criteria presented above, with larger values possible with increased Ω. It can be seen that altering the value of Ω has a small effect on the accuracy of the calculation [note the difference in y-axis values for χ compared with Figs. 2(i)(a) and 2(i)(b)], and the value $\Omega = 5$ was deemed to result in a stable enough propagation.

IV. APPLICATION 2: INDISTINGUISHABLE BOSONS IN A DISPLACED HARMONIC TRAP

The second application of CCSB is to a system composed purely of indistinguishable bosons, with N interacting bosons placed in a harmonic trap displaced from the origin, with $N = 100$ used in the present application. The oscillations in the density are calculated and compared with MCTDHB [21,22] calculations (performed by the authors, using the MCTDHB package [80]). The Hamiltonian (in dimensionless units and distinguishable representation) for this problem consists of a shifted harmonic potential and a two-body interaction term,

$$\hat{H} = \frac{\hat{\mathbf{P}}^2}{2} + \frac{(\hat{\mathbf{Q}} - \xi)^2}{2} + \hat{W}(\mathbf{Q}, \mathbf{Q}'), \tag{32}$$

where $\hat{\mathbf{Q}}$ and $\hat{\mathbf{P}}$ are the position and momentum operators of the N bosons, $\xi = 2.1$ is a parameter that shifts the harmonic potential from the origin, and $\hat{W}$ is the two-body interaction given by the contact interaction

$$\hat{W}(\mathbf{Q}, \mathbf{Q}') = \lambda_0 \delta(\mathbf{Q} - \mathbf{Q}'). \tag{33}$$

The constant λ_0 controls the strength of the interaction, with values of $\lambda_0 = 0.001$ and $\lambda_0 = 0.01$ used in the present application, while $\delta(\mathbf{Q} - \mathbf{Q}')$ is the Dirac δ function. As with Application 1, the Hamiltonian in Eq. (32) must be second quantized and normal ordered before it can be used with CCSB, with

$$\begin{aligned} H_{\mathrm{ord}}(\mathbf{z}_k^*, \mathbf{z}_l) = &\sum_{\alpha=0}^{\Omega} \epsilon^{(\alpha)} z_k^{(\alpha)*} z_l^{(\alpha)} - \sum_{\alpha,\beta=0}^{\Omega} \xi Q^{(\alpha,\beta)} z_k^{(\alpha)*} z_l^{(\beta)} \\ &+ \sum_{\alpha=0}^{\Omega} \frac{\xi^2}{2} z_k^{(\alpha)*} z_l^{(\alpha)} \\ &+ \frac{1}{2} \sum_{\alpha,\beta,\gamma,\zeta=0}^{\Omega} \lambda_0 \delta^{(\alpha,\beta,\gamma,\zeta)} z_k^{(\alpha)*} z_k^{(\beta)*} z_l^{(\zeta)} z_l^{(\gamma)}. \end{aligned} \tag{34}$$

The derivation of the above and evaluation of the matrix elements $Q^{(\alpha,\beta)}$ and $\delta^{(\alpha,\beta,\gamma,\zeta)}$ is shown in Appendix B. The initial sampling of the coherent states and amplitudes is performed in a similar manner to the second-quantized bath of Application 1 and is shown in the following section.

A. Initial conditions for Application 2

The initial Fock state for the system includes all bosons in the ground harmonic state:

$$|\mathbf{n}\rangle = \prod_{\alpha=0}^{\Omega} |n^{(\alpha)}\rangle = |n^{(0)},\ n^{(1)}, \ldots, n^{(\Omega)}\rangle = |100,\ 0, \ldots, 0\rangle\,. \tag{35}$$

As with the second-quantized bath of Application 1, the coherent states are sampled via a gamma distribution like in Eq. (25). The ground state with initial occupation $n^{(\alpha=0)} = 100$ is sampled with compression parameter $\sigma^{(\alpha=0)} = 1.0$ to ensure that the distribution is centered in the correct place, while once more we are free to choose the compression parameter for the excited states with initial occupation $n^{(\alpha>0)} = 0$. Values of $\sigma^{(\alpha>0)} = 10^9$ for $\lambda_0 = 0.001$ and $\sigma^{(\alpha>0)} = 10^7$ for $\lambda_0 = 0.01$ are used, with full details for the determination of these compression parameters shown in the following section.

Initial amplitudes are calculated by projecting the basis onto the initial Fock state in Eq. (35)

$$\langle \mathbf{z}_k(0)|\mathbf{n}\rangle = \sum_{l=1}^{K} D_l(0)\,\langle \mathbf{z}_k(0)|\mathbf{z}_l(0)\rangle\,, \tag{36}$$

where

$$\begin{aligned}\langle \mathbf{z}_k(0)|\mathbf{n}\rangle &= \left\langle \prod_{\alpha=0}^{\Omega} z_k^{(\alpha)}(0)|\mathbf{n})\right\rangle \\ &= \left[\prod_{\alpha=0}^{\Omega} e^{-\frac{|z_k^{(\alpha)}(0)|^2}{2}}\right] \frac{\left(z_k^{(\alpha=0)*}(0)\right)^{100}}{\sqrt{100!}}.\end{aligned} \tag{37}$$

For the MCTDHB calculations, the initial orbitals were constructed from eigenfunctions of the unshifted trap ($\xi = 0$), with the coefficient of one of the orbitals set to 1, while the rest were set to 0. This was chosen for the initial conditions of the MCTDHB calculations rather than propagation in imaginary time to obtain the initial orbitals and coefficients of the ground state [21,22], because we currently do not have an analogous procedure for CCSB due to the instability of trajectories when propagating in imaginary time [81]. This way we ensure that the initial conditions for both methods are the same, and we are testing the propagation accuracy of both methods. In future work we will look at the effect of initial conditions on CCSB, and its comparison to MCTDHB.

B. Results and comparison to multiconfigurational time-dependent Hartree method for bosons

The dynamics are followed by observing the evolution of the density matrix over the course of the calculation, which in CCSB can be evaluated as

$$\begin{aligned}\rho^{(\alpha,\beta)} &= \langle \Psi|\hat{a}^{(\alpha)\dagger}\hat{a}^{(\beta)}|\Psi\rangle \\ &= \sum_{k,l=1}^{K} D_k^* D_l e^{i(S_l - S_k)}\,\langle \mathbf{z}_k|\mathbf{z}_l\rangle\, z_k^{(\alpha)*} z_l^{(\beta)}.\end{aligned} \tag{38}$$

Because the creation and annihilation operators have different interpretations in CCSB and MCTDHB (acting on quantum states vs orbitals), the density matrix in this form also has a different interpretation. Therefore, to compare the two methods on the same footing, the one-body density is evaluated as a function of position, which for CCSB in this application can be calculated by the following:

$$\begin{aligned}\rho(Q) &= \langle \alpha|\rho^{(\alpha,\beta)}|\beta\rangle \\ &= \sum_{\alpha,\beta=0}^{\Omega} \frac{1}{\sqrt{2^\alpha \alpha!}}\left(\frac{1}{\pi}\right)^{1/4} e^{-Q^2/2} He_\alpha(Q)\rho^{(\alpha,\beta)} \\ &\quad \times \frac{1}{\sqrt{2^\beta \beta!}}\left(\frac{1}{\pi}\right)^{1/4} e^{-Q^2/2} He_\beta(Q).\end{aligned} \tag{39}$$

This one-body density is shown as a function of position and time in Fig. 3 for interaction strengths $\lambda_0 = 0.001$ [Fig. 3(i)] and $\lambda_0 = 0.01$ [Fig. 3(ii)], with the MCTDHB calculations in Figs. 3(i)(a) and 3(ii)(a) and CCSB calculations in Figs. 3(i)(b) and 3(ii)(b). The MCTDHB calculations use one orbital for the $\lambda_0 = 0.001$ case, and three orbitals for the $\lambda_0 = 0.01$ case, labeled MCTDHB(1) and MCTDHB(3), respectively. The CCSB calculations use $K = 150$ configurations for both the $\lambda_0 = 0.001$ and $\lambda_0 = 0.01$ cases, with $\Omega = 26$ harmonic-oscillator levels for the $\lambda_0 = 0.001$ case and $\Omega = 25$ harmonic-oscillator levels for the $\lambda_0 = 0.01$ case, with the compression parameters $\sigma^{(\alpha>0)}$ as mentioned in the previous section. It can be seen that the MCTDHB and CCSB calculations of the one-body density compare well to one another, illustrating the oscillations in the bosonic cloud due to the trap displacement.

As well as the density being subject to oscillations as a function of the trap displacement, it also exhibits breathing oscillations, which may not be immediately apparent from Fig. 3. To illustrate these, we plot the variance in the one-body density as a function of time

$$\langle Q\rangle = \int Q^2\rho(Q)dQ - \left(\int Q\rho(Q)dQ\right)^2, \tag{40}$$

which is shown in Fig. 4, with the interaction strengths $\lambda_0 = 0.001$ in Fig. 4(i) and $\lambda_0 = 0.01$ in Fig. 4(ii). It can immediately be seen that the stronger interaction strength produces larger breathing oscillations, which is not as easy to see in Fig. 3. Furthermore, the breathing oscillations in Fig. 4 serve to determine the convergence of the methods: MCTDHB with respect to the number of orbitals; and CCSB with respect to $\sigma^{(\alpha>0)}$, K, and Ω. A portion of the peak of the density variance at $\sim$8 a.u. is highlighted to clearly illustrate any discrepancies that may be difficult to distinguish. As with Application 1, the accuracy and convergence of the CCSB calculation may also be determined from the conservation of norm and particle number, which is shown in Fig. 5.

For $\lambda_0 = 0.001$, the MCTDHB calculations using 1, 3, and 4 orbitals demonstrate equivalent breathing oscillations in Fig. 4(i)(a), while there appears to be an anomalous result for MCTDHB with two orbitals. The authors are unsure of the reason for this, which may be best left for a future MCTDHB study; however, we regard the MCTDHB(1) as being fully converged and use this to compare with the CCSB calculations in Figs. 4(i)(b)–4(i)(d), as well as in Fig. 3(i). An MCTDHB calculation with one orbital is equivalent to the GPE [82], so these dynamics are at the mean-field level.

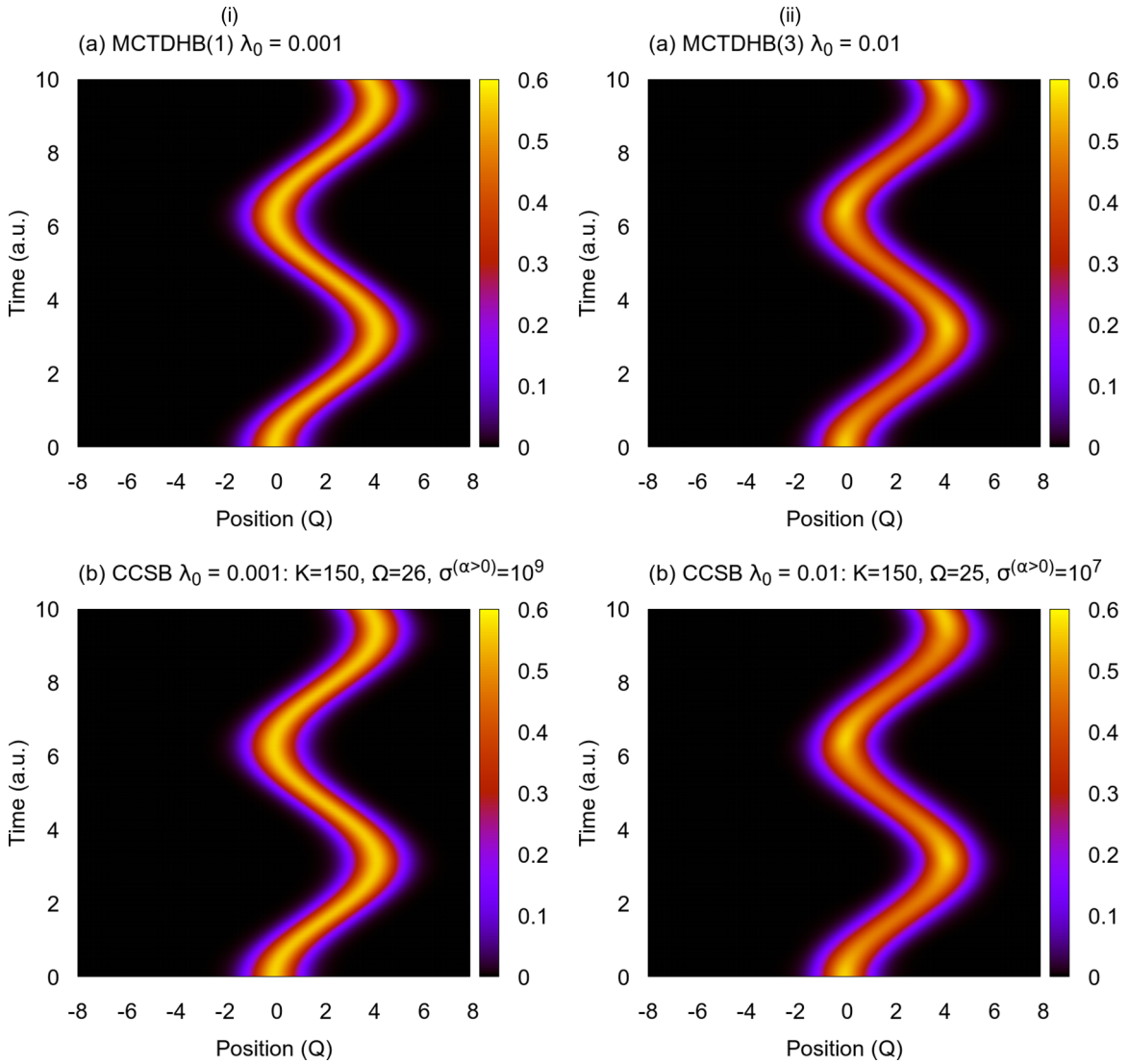

FIG. 3. Spacetime representation of the evolution of the one-body density for (a) MCTDHB and (b) CCSB calculations of Application 2 with interaction strengths (i) $\lambda_0 = 0.001$ and (ii) $\lambda_0 = 0.01$.

In Fig. 4(i)(b) we alter the value of the compression parameter $\sigma^{(\alpha>0)}$, while keeping the number of configurations fixed at $K = 150$, and the number of harmonic-oscillator levels fixed at $\Omega = 26$. There appears to be little difference in the breathing oscillations for different values of $\sigma^{(\alpha>0)}$, although the highlighted peak at ∼8 a.u. demonstrates small discrepancies between the MCTDHB calculation and $\sigma^{(\alpha>0)} = 10^6$ and $\sigma^{(\alpha>0)} = 10^7$, while $\sigma^{(\alpha>0)} = 10^8$ and $\sigma^{(\alpha>0)} = 10^9$ superimpose on the MCTDHB result. The conservation of norm and particle number for different values of $\sigma^{(\alpha>0)}$ is shown in Fig. 5(i)(a), where $\sigma^{(\alpha>0)} = 10^8$ and $\sigma^{(\alpha>0)} = 10^9$ superimpose upon a value of the norm of 1, and particle number 100, as should be expected. We keep $\sigma^{(\alpha>0)} = 10^9$ for the remaining calculations. This is much larger than the compression parameter used in Application 1; however, much fewer configurations are used in this application, and the compression parameter necessary also depends upon the problem studied, and how the dynamics affect the motion of the basis.

In Fig. 4(i)(c) we alter the value of K while keeping $\sigma^{(\alpha>0)}$ and Ω fixed. Altering the value of the compression parameter for different values of K was not necessary like in Application 1, as a stable basis was able to be formed. We observe very little discrepancy between the different CCSB calculations and MCTDHB, and the norm and particle number conservation for $K = 150$ and $K = 200$ are very similar in Fig. 5(i)(b). We therefore regard $K = 150$ as being fully converged.

In Fig. 4(i)(d) we alter the value of Ω and keep K and $\sigma^{(\alpha>0)}$ fixed. As with the above, altering the value of $\sigma^{(\alpha>0)}$ was not necessary because a stable basis was able to be formed each time. Larger discrepancies between the CCSB calculations and the MCTDHB result are seen in this panel, indicating that the choice of Ω has the largest influence on this calculation. The results for $\Omega = 25$ and $\Omega = 26$ superimpose, indicating that the calculation is converged by this point. The conservation of norm and particle number for both of these calculations is also similar in Fig. 5(i)(c).

Turning to the larger interaction strength of $\lambda_0 = 0.01$, we follow the same approach as above in determining the accuracy and convergence of the calculations. Initially, in Fig. 4(ii)(a), the MCTDHB calculations with one and two

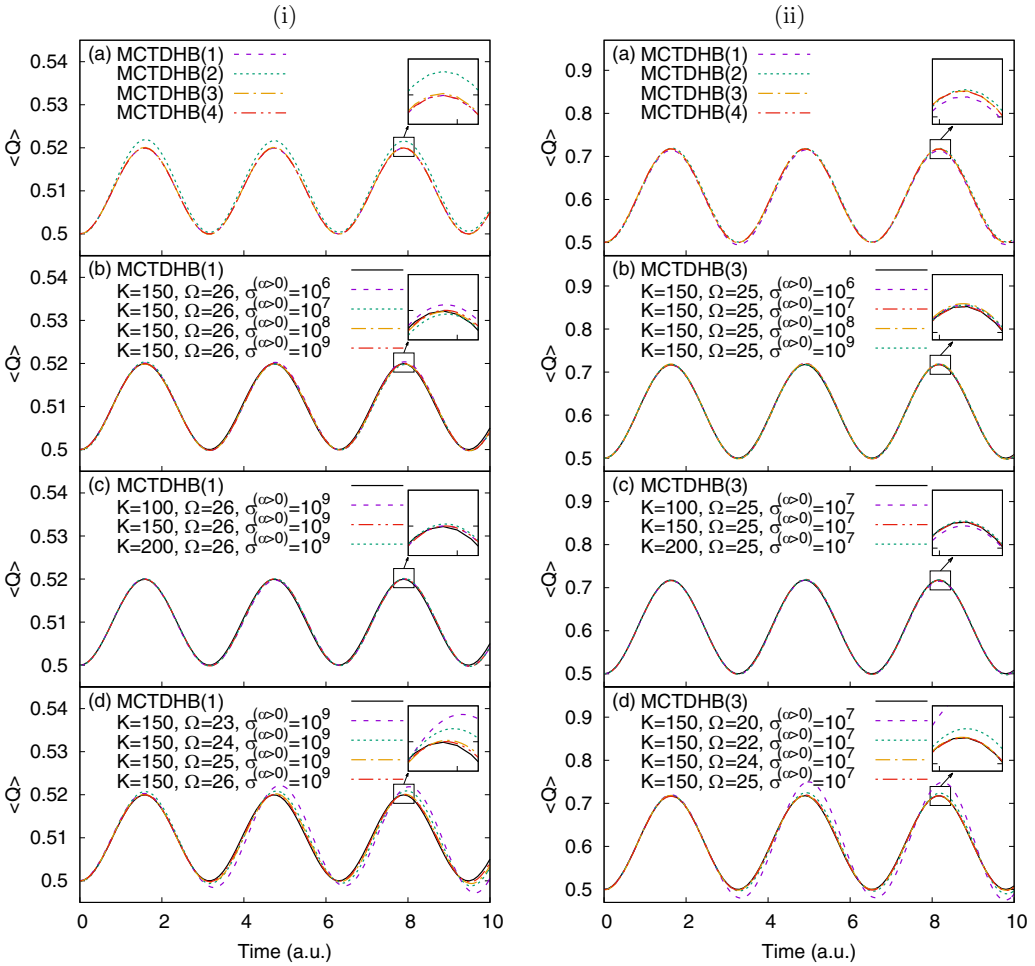

FIG. 4. Variance of the one-body density $\langle Q \rangle$ for Application 2 with two-body interaction strength (i) $\lambda_0 = 0.001$ and (ii) $\lambda_0 = 0.01$. Panels (a) show the MCTDHB calculations with different numbers of orbitals, and the converged result is used to compare with CCSB calculations with different values of (b) compression parameter for coherent-state sampling of the harmonic-oscillator levels with zero initial occupation $\sigma^{(\alpha>0)}$, (c) configurations K, and (d) harmonic-oscillator levels in the basis Ω.

orbitals exhibit minor differences with respect to those with three and four orbitals, shown in the highlighted portion of the figure, so we regard the MCTDHB(3) calculation as our fully converged reference point. At this level of interaction strength, an above-mean-field description is therefore necessary. We admit that the discrepancy between these MCTDHB calculations is not very large; however, a similar study in Ref. [31] also illustrated minor differences in breathing dynamics for MCTDHB calculations with different numbers of orbitals.

In Fig. 4(ii)(b) we alter the value of the compression parameter $\sigma^{(\alpha>0)}$, while keeping the number of configurations fixed at $K = 150$, and the number of harmonic-oscillator levels fixed at $\Omega = 25$. All the calculations superimpose, and there is even less discrepancy than in the $\lambda_0 = 0.001$ case. For the remaining calculations we choose a compression parameter of $\sigma^{(\alpha>0)} = 10^7$ because this demonstrates the best norm and particle number conservation in Fig. 5(ii)(a).

In Fig. 4(ii)(c) we alter the value of K while keeping $\sigma^{(\alpha>0)}$ and Ω fixed. There are minor differences between the $K = 100$ calculation and the $K = 150$ and $K = 200$ calculations, the latter of which superimpose on the MCTDHB result. The norm and particle number conservation of the $K = 150$ and $K = 200$ calculations are very similar in Fig. 5(ii)(b), therefore we regard the $K = 150$ result as being fully converged.

In Fig. 4(ii)(d) we alter the value of Ω and keep K and $\sigma^{(\alpha>0)}$ fixed. As with the $\lambda_0 = 0.001$ calculations, this has the largest effect on the breathing oscillations, with $\Omega = 20$ and $\Omega = 22$ being insufficient to describe them accurately, while the $\Omega = 24$ and $\Omega = 25$ cases superimpose upon the MCTDHB result. The norm and particle number conservation of the $\Omega = 24$ result, shown in Fig. 5(ii)(c) is not as good as the $\Omega = 25$ result, which is why we choose the latter as our most accurate calculation.

The above demonstrates that CCSB is able to reproduce MCTDHB calculations in both the mean-field and multi-orbital fully quantum regimes, with similar levels of theory for the CCSB calculations in each regime. We have also shown that the method converges appropriately with respect to the K and Ω parameters, this it is stable with respect to norm and particle number conservation, and that appropriate choice of the compression parameter $\sigma^{(\alpha>0)}$ for initial sampling of the coherent-state basis is necessary, like in Application 1.

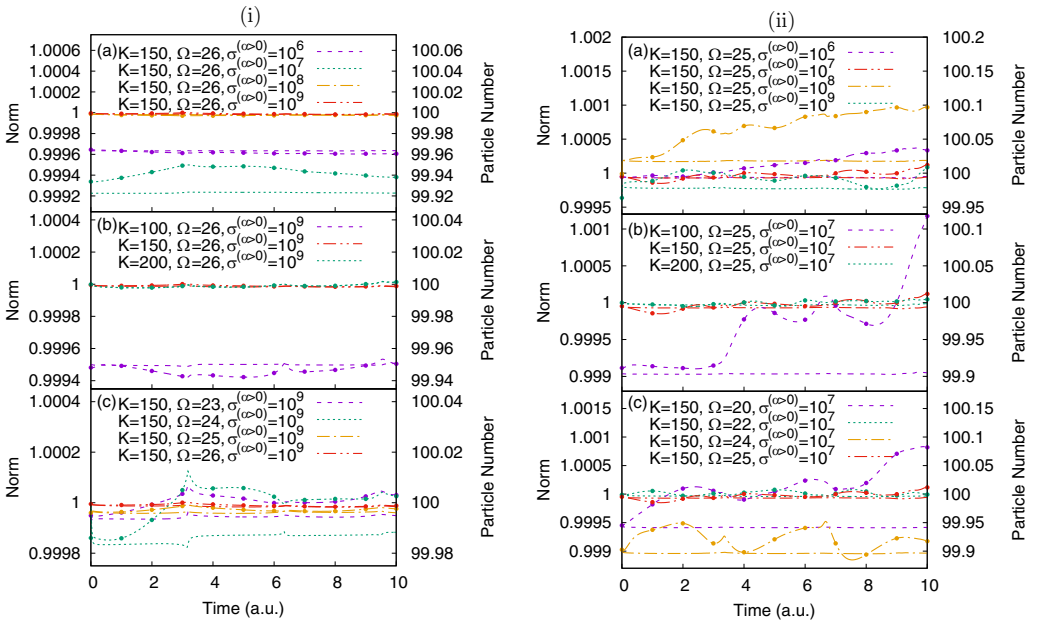

FIG. 5. Norm (dashed-dotted lines without circles) and particle number (dashed-dotted lines with circles) for CCSB calculations of Application 2 with two-body interaction strength (i) $\lambda_0 = 0.001$ and (ii) $\lambda_0 = 0.01$ with different values of (a) compression parameter for coherent-state sampling of the harmonic-oscillator levels with zero initial occupation $\sigma^{(\alpha>0)}$, (b) configurations K, and (c) harmonic-oscillator levels in the basis Ω.

V. CONCLUSIONS

In this work the CCS method has been straightforwardly applied to the investigation of indistinguishable bosons, as MCTDH and ML-MCTDH have been, and the method dubbed CCSB. Instead of the coherent-state basis functions being used to represent individual particles like in the standard distinguishable representation of CCS, in CCSB they are used as a basis for number occupation of quantum states in the second-quantization Fock state formalism.

Two example model Hamiltonians have been studied, demonstrating the accuracy of the method by comparing with fully quantum benchmarks. In the first example, CCSB was applied to the system-bath asymmetric double-well tunneling problem previously studied in Refs. [72–75,78,79] in distinguishable representation. Because the bath is comprised of oscillators of the same frequency, they were treated as indistinguishable and the bath portion of the Hamiltonian second quantized. The system tunneling portion of the Hamiltonian was kept in distinguishable representation, therefore this first application was a hybrid of standard CCS and CCSB. This does not pose a problem however, because the working equations for trajectories and time dependence of amplitudes are the same in each. This may also be thought of as a system with a bosonic bath and an impurity, opening up the possibility of the method studying multi-atomic Bose-Einstein condensates [64], spinor Bose-Einstein condensates [65], dark-bright solitons [66], and Bose polarons [67]. The previously studied 20D, quadratic system-bath coupling with constant $\lambda = 0.1$ case [72–75,78,79] was investigated, and the second-quantized bath required $\Omega = 5$ harmonic-oscillator levels in the basis, thus the dimensionality of the problem was reduced from 20 to 6. The CCSB calculation was in much better agreement with a benchmark result [79] on the system than all other methods that have studied the problem.

In the second example, a model Hamiltonian for a system of 100 bosons in a shifted harmonic trap was studied, the one-body density has been calculated, as well as its variance, to demonstrate the breathing oscillations of the density. Matrix elements of two-body operators had to be calculated, as is common for interacting condensates, and these may be computed analytically by CCSB. The density oscillations were calculated at two different two-body interaction strengths and compared with MCTDHB benchmark calculations. The weaker interaction strength was able to be described by MCTDHB with one orbital, such that it was equivalent to the GPE mean-field theory, while the stronger interaction strength required MCTDHB with three orbitals, and was thus fully quantum, taking correlations into account and going beyond the mean-field approach. CCSB was able to reproduce both results with similar levels of theory, providing motivation for further study on more challenging Bose-Einstein condensate systems. In particular, future avenues of research for CCSB in this vein include more complicated Bose-Einstein condensate problems, such as that in Ref. [22] of a condensate in a single-well trap that is deformed into a double well, like that observed in experimental bosonic Josephson junctions [70,71]. We also wish to consider condensates in multiwell traps, such as a multisite version of the Bose-Hubbard model studied in Ref. [61], and other interesting systems that have previously been studied by ML-MCTDHB [45–52].

Both applications have demonstrated that the CCSB method converges with the number of configurations K and number of quantum states included in the basis Ω. We have

also demonstrated that appropriate sampling of the initial coherent states via a compression parameter σ is necessary to ensure a reliable and accurate calculation. Further developments of the method that we envisage in the future include development of methods to generate initial conditions, as imaginary time propagation is unstable with trajectories; incorporation of SU(n) coherent states, as demonstrated in Ref. [83], and the combination of the method with one to treat identical fermions [84] to study Bose-Fermi mixtures, as has been carried out by MCTDH [85] and ML-MCTDH [86] previously.

The data generated in this work that are shown in the figures are available, along with the program code used to generate the data [87].

ACKNOWLEDGMENTS

J.A.G. has been supported by EPSRC Grant No. EP/N007549/1, as well as the University Research Scholarship from the University of Leeds, and funding from the School of Chemistry, University of Leeds. D.V.S acknowledges the support of the EPSRC, Grant No. EP/P021123/1. J.A.G. would like to thank A. Streltsov for demonstration of the use of the MCTDHB program, alongside helpful discussions. J.A.G would also like to thank L. Chen for reading through the paper and suggesting modifications. J.A.G. and D.V.S gratefully acknowledge V. Batista, S. Habershon, and M. Saller for providing their data. This work was undertaken on ARC2 and ARC3, part of the High Performance Computing facilities at the University of Leeds, UK.

APPENDIX A: SECOND QUANTIZATION AND NORMAL ORDERING OF HAMILTONIAN FOR APPLICATION 1

Using the definition of a second-quantized Hamiltonian in Eq. (17) in the main text, Eq. (18) may be written as

$$\begin{aligned}\hat{H} &= \frac{\hat{p}^{(m=1)^2}}{2} - \frac{\hat{q}^{(m=1)^2}}{2} + \frac{\hat{q}^{(m=1)^4}}{16\eta} + \left[\sum_{\alpha,\beta=0}^{\Omega} \langle\alpha|\frac{\hat{\mathbf{P}}^2}{2} + \frac{\hat{\mathbf{Q}}^2}{2}|\beta\rangle\, \hat{a}^{(\alpha)\dagger}\hat{a}^{(\beta)}\right] + \frac{\lambda\hat{q}^{(m=1)}}{2}\left[\sum_{\alpha,\beta=0}^{\Omega} \langle\alpha|\hat{\mathbf{Q}}^2|\beta\rangle\, \hat{a}^{(\alpha)\dagger}\hat{a}^{(\beta)}\right] \\ &= \frac{\hat{p}^{(m=1)^2}}{2} - \frac{\hat{q}^{(m=1)^2}}{2} + \frac{\hat{q}^{(m=1)^4}}{16\eta} + \left[\sum_{\alpha=0}^{\Omega} \langle\alpha|\frac{\hat{\mathbf{P}}^2}{2} + \frac{\hat{\mathbf{Q}}^2}{2}|\alpha\rangle\, \hat{a}^{(\alpha)\dagger}\hat{a}^{(\alpha)}\right] + \frac{\lambda\hat{q}^{(m=1)}}{2}\left[\sum_{\alpha,\beta=0}^{\Omega} Q^{(\alpha,\beta)^2}\hat{a}^{(\alpha)\dagger}\hat{a}^{(\beta)}\right] \\ &= \frac{\hat{p}^{(m=1)^2}}{2} - \frac{\hat{q}^{(m=1)^2}}{2} + \frac{\hat{q}^{(m=1)^4}}{16\eta} + \left[\sum_{\alpha=0}^{\Omega} \epsilon^{(\alpha)}\hat{a}^{(\alpha)\dagger}\hat{a}^{(\alpha)}\right] + \frac{\lambda\hat{q}^{(m=1)}}{2}\left[\sum_{\alpha,\beta=0}^{\Omega} Q^{(\alpha,\beta)^2}\hat{a}^{(\alpha)\dagger}\hat{a}^{(\beta)}\right]. \end{aligned} \tag{A1}$$

The quantum states $|\alpha\rangle$ and $|\beta\rangle$ are those of the harmonic oscillator with α and β being the numbers of quanta, and the equality for $\langle\alpha|\frac{\hat{\mathbf{P}}^2}{2} + \frac{\hat{\mathbf{Q}}^2}{2}|\beta\rangle$ in the second step follows because this is nonzero with eigenvalue $\epsilon^{(\alpha)}$ only when $\alpha = \beta$. The sums are from the ground level $\alpha = 0$ to some upper level Ω. In principle, one should choose $\Omega = \infty$ for a complete description of the bath; however, in practice additional oscillator levels may simply be added on until a converged result is achieved. The position and momentum operators of the tunneling mode have been explicitly labeled with $(m = 1)$ to distinguish them from the α-labeling scheme of the second-quantized bath modes.

The matrix $Q^{(\alpha,\beta)^2}$ is evaluated as

$$\langle\alpha|\hat{\mathbf{Q}}^2|\beta\rangle = \begin{cases} \frac{1}{2}\sqrt{(\alpha+2)(\alpha+1)} & \text{if } \alpha = \beta - 2 \\ \frac{1}{2}\sqrt{\alpha(\alpha-1)} & \text{if } \alpha = \beta + 2 \\ \epsilon^{(\alpha)} & \text{if } \alpha = \beta \\ 0 & \text{otherwise.} \end{cases} \tag{A2}$$

As this matrix is nonzero only for quanta $\alpha = \beta$ and $\alpha = \beta \pm 2$, and we may say that all bath modes are initially in the ground harmonic-oscillator level ($\alpha = 0$) because they are at the origin in distinguishable representation (previously assumed in the benchmark calculation [79]), only harmonic-oscillator levels with even numbers of quanta will be included and the bottom line of Eq. (A1) is written as

$$\hat{H} = \frac{\hat{p}^{(m=1)^2}}{2} - \frac{\hat{q}^{(m=1)^2}}{2} + \frac{\hat{q}^{(m=1)^4}}{16\eta} + \left[\sum_{\alpha=0}^{\Omega} \epsilon^{(2\alpha)}\hat{a}^{(2\alpha)\dagger}\hat{a}^{(2\alpha)}\right] + \frac{\lambda\hat{q}^{(m=1)}}{2}\left[\sum_{\alpha,\beta=0}^{\Omega} Q^{(2\alpha,2\beta)^2}\hat{a}^{(2\alpha)\dagger}\hat{a}^{(2\beta)}\right]. \tag{A3}$$

The relationship between the creation and annihilation operators and $\hat{q}$ and $\hat{p}$ given in Eq. (3) may then be used in Eq. (A3) alongside the relationships in Eqs. (2) and (6) to give Eq. (19).

APPENDIX B: SECOND QUANTIZATION OF HAMILTONIAN FOR APPLICATION 2

Using the definition of a second-quantized Hamiltonian in Eq. (17) in the main text, Eq. (32) may be written as

$$\begin{aligned}\hat{H} &= \sum_{\alpha,\beta=0}^{\Omega} \langle\alpha|\frac{\hat{\mathbf{P}}^2}{2}+\frac{\hat{\mathbf{Q}}^2}{2}|\beta\rangle\,\hat{a}^{(\alpha)\dagger}\hat{a}^{(\beta)} - \sum_{\alpha,\beta=0}^{\Omega}\langle\alpha|\xi\hat{\mathbf{Q}}|\beta\rangle\,\hat{a}^{(\alpha)\dagger}\hat{a}^{(\beta)} + \sum_{\alpha,\beta=0}^{\Omega}\langle\alpha|\frac{\xi^2}{2}|\beta\rangle\,\hat{a}^{(\alpha)\dagger}\hat{a}^{(\beta)} \\ &\quad + \frac{1}{2}\sum_{\alpha,\beta,\gamma,\zeta=0}^{\Omega}\langle\alpha,\beta|\lambda_0\delta(\mathbf{Q}-\mathbf{Q}')|\gamma,\zeta\rangle\,\hat{a}^{(\alpha)\dagger}\hat{a}^{(\beta)\dagger}\hat{a}^{(\zeta)}\hat{a}^{(\gamma)} \\ &= \sum_{\alpha=0}^{\Omega}\langle\alpha|\frac{\hat{\mathbf{P}}^2}{2}+\frac{\hat{\mathbf{Q}}^2}{2}|\alpha\rangle\,\hat{a}^{(\alpha)\dagger}\hat{a}^{(\alpha)} - \sum_{\alpha,\beta=0}^{\Omega}\langle\alpha|\xi\hat{\mathbf{Q}}|\beta\rangle\,\hat{a}^{(\alpha)\dagger}\hat{a}^{(\beta)} \\ &\quad + \sum_{\alpha=0}^{\Omega}\langle\alpha|\frac{\xi^2}{2}|\alpha\rangle\,\hat{a}^{(\alpha)\dagger}\hat{a}^{(\alpha)} + \frac{1}{2}\sum_{\alpha,\beta,\gamma,\zeta=0}^{\Omega}\langle\alpha,\beta|\lambda_0\delta(\mathbf{Q}-\mathbf{Q}')|\gamma,\zeta\rangle\,\hat{a}^{(\alpha)\dagger}\hat{a}^{(\beta)\dagger}\hat{a}^{(\zeta)}\hat{a}^{(\gamma)} \\ &= \sum_{\alpha=0}^{\Omega}\epsilon^{(\alpha)}\hat{a}^{(\alpha)\dagger}\hat{a}^{(\alpha)} - \sum_{\alpha,\beta=0}^{\Omega}\xi Q^{(\alpha,\beta)}\hat{a}^{(\alpha)\dagger}\hat{a}^{(\beta)} + \sum_{\alpha=0}^{\Omega}\frac{\xi^2}{2}\hat{a}^{(\alpha)\dagger}\hat{a}^{(\alpha)} \\ &\quad + \frac{1}{2}\sum_{\alpha,\beta,\gamma,\zeta=0}^{\Omega}\lambda_0\delta^{(\alpha,\beta,\gamma,\zeta)}\hat{a}^{(\alpha)\dagger}\hat{a}^{(\beta)\dagger}\hat{a}^{(\zeta)}\hat{a}^{(\gamma)}. \end{aligned} \tag{B1}$$

The relationships in Eqs. (2) and (6) may then be used with Eq. (B1) to give Eq. (34). In Eq. (B1), $\epsilon^{(\alpha)}$ is the eigenvalue of the harmonic oscillator for state $|\alpha\rangle$, and $Q^{(\alpha,\beta)}$ is a matrix given by

$$Q^{(\alpha,\beta)} = \langle\alpha|\hat{\mathbf{Q}}|\beta\rangle = \begin{cases}\sqrt{\frac{\alpha}{2}} & \alpha=\beta+1\\ \sqrt{\frac{\beta}{2}} & \beta=\alpha+1\\ 0 & \text{otherwise.}\end{cases} \tag{B2}$$

Evaluation of the $\delta^{(\alpha,\beta,\gamma,\zeta)}$ matrix is slightly more involved, because it is required to solve the integral

$$\begin{aligned}\delta^{(\alpha,\beta,\gamma,\zeta)} = \langle\alpha,\beta|\delta(\mathbf{Q}-\mathbf{Q}')|\gamma,\zeta\rangle &= \int_{-\infty}^{+\infty}\int_{-\infty}^{+\infty}\frac{1}{\sqrt{2^\alpha\alpha!}}\left(\frac{1}{\pi}\right)^{1/4}e^{-\mathbf{Q}^2/2}He^{(\alpha)}(\mathbf{Q})\frac{1}{\sqrt{2^\beta\beta!}}\left(\frac{1}{\pi}\right)^{1/4}e^{-\mathbf{Q}^2/2}He^{(\beta)}(\mathbf{Q}') \\ &\quad\times\delta(\mathbf{Q}-\mathbf{Q}')\frac{1}{\sqrt{2^\gamma\gamma!}}\left(\frac{1}{\pi}\right)^{1/4}e^{-\mathbf{Q}^2/2}He^{(\gamma)}(\mathbf{Q})\frac{1}{\sqrt{2^\zeta\zeta!}}\left(\frac{1}{\pi}\right)^{1/4}e^{-\mathbf{Q}^2/2}He^{(\zeta)}(\mathbf{Q}')d\mathbf{Q}d\mathbf{Q}', \end{aligned} \tag{B3}$$

where $He^{(\alpha)}(\mathbf{Q})$ is a Hermite polynomial of order α. However, an analytic solution is possible, and the above may be simplified by using the relationship

$$\int_{-\infty}^{+\infty} f(x')\delta(x-x')dx' = f(x) \tag{B4}$$

and like terms collated to obtain

$$\delta^{(\alpha,\beta,\gamma,\zeta)} = \frac{1}{\pi\sqrt{2^{(\alpha+\beta+\gamma+\zeta)}\alpha!\beta!\gamma!\zeta!}}\int_{-\infty}^{+\infty}e^{-2\mathbf{Q}^2}He^{(\alpha)}(\mathbf{Q})He^{(\beta)}(\mathbf{Q})He^{(\gamma)}(\mathbf{Q})He^{(\zeta)}(\mathbf{Q})d\mathbf{Q}. \tag{B5}$$

This will only be nonzero if the integrand is an even function, so the product of Hermite polynomials can only have even powers of $\mathbf{Q}$:

$$\delta^{(\alpha,\beta,\gamma,\zeta)} = \frac{1}{\pi\sqrt{2^{\alpha+\beta+\gamma+\zeta}\alpha!\beta!\gamma!\zeta!}}\int_{-\infty}^{+\infty}e^{-2\mathbf{Q}^2}\sum_{\tau=0}^{(\alpha+\beta+\gamma+\zeta)/2}c_{2\tau}\mathbf{Q}^{2\tau}d\mathbf{Q}, \tag{B6}$$

where $c_{2\tau}$ is a constant obtained from the product of Hermite polynomial coefficients. Using the identity

$$\int_{-\infty}^{+\infty}x^{2n}e^{-\frac{1}{2}ax^2}dx = \sqrt{\frac{2\pi}{a}}\frac{1}{a^n}(2n-1)!!\ \text{for}\ n>0 \tag{B7}$$

combined with a Gaussian integral for $\tau = 0$, Eq. (B6) can be evaluated as

$$\delta^{(\alpha,\beta,\gamma,\zeta)} = \frac{1}{\pi\sqrt{2^{\alpha+\beta+\gamma+\zeta}\alpha!\beta!\gamma!\zeta!}}\left[\sqrt{\frac{\pi}{2}}c_0 + \sum_{\tau=1}^{(\alpha+\beta+\gamma+\zeta)/2} c_{2\tau}\sqrt{\frac{\pi}{2}}\frac{1}{4^\tau}(2\tau-1)!!\right]. \tag{B8}$$

We note that an alternative method of calculating the $\delta^{(\alpha,\beta,\gamma,\zeta)}$ matrix elements exists by using Gauss-Hermite quadrature [88]; however, our approach was sufficiently efficient.

[1] M. H. Anderson, J. R. Ensher, M. R. Matthews, C. E. Wieman, and E. A. Cornell, Science **269**, 198 (1995).
[2] C. C. Bradley, C. A. Sackett, J. J. Tollett, and R. G. Hulet, Phys. Rev. Lett. **75**, 1687 (1995).
[3] K. B. Davis, M. O. Mewes, M. R. Andrews, N. J. van Druten, D. S. Durfee, D. M. Kurn, and W. Ketterle, Phys. Rev. Lett. **75**, 3969 (1995).
[4] C. Orzel, A. K. Tuchman, M. L. Fenselau, M. Yasuda, and M. A. Kasevich, Science **291**, 2386 (2001).
[5] M. Albiez, R. Gati, J. Fölling, S. Hunsmann, M. Cristiani, and M. K. Oberthaler, Phys. Rev. Lett. **95**, 010402 (2005).
[6] S. Levy, E. Lahoud, I. Shomroni, and J. Steinhauer, Nature (London) **449**, 579 (2007).
[7] M. R. Matthews, B. P. Anderson, P. C. Haljan, D. S. Hall, C. E. Wieman, and E. A. Cornell, Phys. Rev. Lett. **83**, 2498 (1999).
[8] K. W. Madison, F. Chevy, W. Wohlleben, and J. Dalibard, Phys. Rev. Lett. **84**, 806 (2000).
[9] S. Burger, K. Bongs, S. Dettmer, W. Ertmer, K. Sengstock, A. Sanpera, G. V. Shlyapnikov, and M. Lewenstein, Phys. Rev. Lett. **83**, 5198 (1999).
[10] J. Denschlag, J. E. Simsarian, D. L. Feder, C. W. Clark, L. A. Collins, J. Cubizolles, L. Deng, E. W. Hagley, K. Helmerson, W. P. Reinhardt, S. L. Rolston, B. I. Schneider, and W. D. Phillips, Science **287**, 97 (2000).
[11] E. P. Gross, Nuovo Cimento **20**, 454 (1961).
[12] L. P. Pitaevskii, Sov. Phys. JETP-USSR **13**, 451 (1961).
[13] A. Smerzi, S. Fantoni, S. Giovanazzi, and S. R. Shenoy, Phys. Rev. Lett. **79**, 4950 (1997).
[14] V. M. Pérez-García, H. Michinel, J. I. Cirac, M. Lewenstein, and P. Zoller, Phys. Rev. A **56**, 1424 (1997).
[15] S. Raghavan, A. Smerzi, S. Fantoni, and S. R. Shenoy, Phys. Rev. A **59**, 620 (1999).
[16] W. Bao, D. Jaksch, and P. A. Markowich, J. Comput. Phys. **187**, 318 (2003).
[17] Z. X. Liang, Z. D. Zhang, and W. M. Liu, Phys. Rev. Lett. **94**, 050402 (2005).
[18] D. Ananikian and T. Bergeman, Phys. Rev. A **73**, 013604 (2006).
[19] A. J. Leggett, Rev. Mod. Phys. **73**, 307 (2001).
[20] A. Minguzzi, S. Succi, F. Toschi, M. Tosi, and P. Vignolo, Phys. Rep. **395**, 223 (2004).
[21] A. I. Streltsov, O. E. Alon, and L. S. Cederbaum, Phys. Rev. Lett. **99**, 030402 (2007).
[22] O. E. Alon, A. I. Streltsov, and L. S. Cederbaum, Phys. Rev. A **77**, 033613 (2008).
[23] A. I. Streltsov, O. E. Alon, and L. S. Cederbaum, Phys. Rev. Lett. **100**, 130401 (2008).
[24] A. I. Streltsov, O. E. Alon, and L. S. Cederbaum, Phys. Rev. A **80**, 043616 (2009).
[25] A. I. Streltsov, O. E. Alon, and L. S. Cederbaum, J. Phys. B: At., Mol. Opt. Phys. **42**, 091004 (2009).
[26] A. U. J. Lode, A. I. Streltsov, O. E. Alon, H.-D. Meyer, and L. S. Cederbaum, J. Phys. B: At., Mol. Opt. Phys. **42**, 044018 (2009).
[27] K. Sakmann, A. I. Streltsov, O. E. Alon, and L. S. Cederbaum, Phys. Rev. Lett. **103**, 220601 (2009).
[28] K. Sakmann, A. I. Streltsov, O. E. Alon, and L. S. Cederbaum, Phys. Rev. A **82**, 013620 (2010).
[29] A. I. Streltsov, O. E. Alon, and L. S. Cederbaum, Phys. Rev. Lett. **106**, 240401 (2011).
[30] A. I. Streltsov, K. Sakmann, O. E. Alon, and L. S. Cederbaum, Phys. Rev. A **83**, 043604 (2011).
[31] A. U. J. Lode, K. Sakmann, O. E. Alon, L. S. Cederbaum, and A. I. Streltsov, Phys. Rev. A **86**, 063606 (2012).
[32] A. I. Streltsov, Phys. Rev. A **88**, 041602(R) (2013).
[33] R. Beinke, S. Klaiman, L. S. Cederbaum, A. I. Streltsov, and O. E. Alon, Phys. Rev. A **92**, 043627 (2015).
[34] L. Cao, S. Krönke, O. Vendrell, and P. Schmelcher, J. Chem. Phys. **139**, 134103 (2013).
[35] S. Krönke, L. Cao, O. Vendrell, and P. Schmelcher, New J. Phys. **15**, 063018 (2013).
[36] J. M. Schurer, A. Negretti, and P. Schmelcher, Phys. Rev. Lett. **119**, 063001 (2017).
[37] K. Keiler and P. Schmelcher, New J. Phys. **20**, 103042 (2018).
[38] S. I. Mistakidis, A. G. Volosniev, N. T. Zinner, and P. Schmelcher, arXiv:1809.01889 [Phys. Rev. A (to be published)].
[39] S. Mistakidis, G. Katsimiga, G. Koutentakis, T. Busch, and P. Schmelcher, Phys. Rev. Lett. **122**, 183001 (2019).
[40] G. C. Katsimiga, S. I. Mistakidis, G. M. Koutentakis, P. G. Kevrekidis, and P. Schmelcher, Phys. Rev. A **98**, 013632 (2018).
[41] S. I. Mistakidis, G. C. Katsimiga, P. G. Kevrekidis, and P. Schmelcher, New J. Phys. **20**, 043052 (2018).
[42] G. C. Katsimiga, G. M. Koutentakis, S. I. Mistakidis, P. G. Kevrekidis, and P. Schmelcher, New J. Phys. **19**, 073004 (2017).
[43] S. Krönke and P. Schmelcher, Phys. Rev. A **91**, 053614 (2015).
[44] G. C. Katsimiga, S. I. Mistakidis, G. M. Koutentakis, P. G. Kevrekidis, and P. Schmelcher, New J. Phys. **19**, 123012 (2017).
[45] S. I. Mistakidis, L. Cao, and P. Schmelcher, J. Phys. B: At., Mol. Opt. Phys. **47**, 225303 (2014).
[46] S. I. Mistakidis, L. Cao, and P. Schmelcher, Phys. Rev. A **91**, 033611 (2015).
[47] S. I. Mistakidis, T. Wulf, A. Negretti, and P. Schmelcher, J. Phys. B: At., Mol. Opt. Phys. **48**, 244004 (2015).
[48] S. I. Mistakidis and P. Schmelcher, Phys. Rev. A **95**, 013625 (2017).

[49] G. M. Koutentakis, S. I. Mistakidis, and P. Schmelcher, Phys. Rev. A **95**, 013617 (2017).
[50] J. Neuhaus-Steinmetz, S. I. Mistakidis, and P. Schmelcher, Phys. Rev. A **95**, 053610 (2017).
[51] S. Mistakidis, G. Koutentakis, and P. Schmelcher, Chem. Phys. **509**, 106 (2018).
[52] T. Plaßmann, S. I. Mistakidis, and P. Schmelcher, J. Phys. B: At., Mol. Opt. Phys. **51**, 225001 (2018).
[53] H.-D. Meyer, U. Manthe, and L. Cederbaum, Chem. Phys. Lett. **165**, 73 (1990).
[54] H. Wang and M. Thoss, J. Chem. Phys. **119**, 1289 (2003).
[55] U. Manthe, J. Chem. Phys. **128**, 164116 (2008).
[56] D. V. Shalashilin and M. S. Child, J. Chem. Phys. **113**, 10028 (2000).
[57] D. V. Shalashilin and M. S. Child, Chem. Phys. **304**, 103 (2004).
[58] D. V. Shalashilin and M. S. Child, J. Chem. Phys. **119**, 1961 (2003).
[59] D. V. Shalashilin and M. S. Child, J. Chem. Phys. **128**, 054102 (2008).
[60] L. Simon and W. T. Strunz, Phys. Rev. A **89**, 052112 (2014).
[61] S. Ray, P. Ostmann, L. Simon, F. Grossmann, and W. T. Strunz, J. Phys. A: Math. Theor. **49**, 165303 (2016).
[62] M. S. Child and D. V. Shalashilin, J. Chem. Phys. **118**, 2061 (2003).
[63] D. V. Shalashilin and M. S. Child, J. Chem. Phys. **121**, 3563 (2004).
[64] G. Modugno, M. Modugno, F. Riboli, G. Roati, and M. Inguscio, Phys. Rev. Lett. **89**, 190404 (2002).
[65] Y. Kawaguchi and M. Ueda, Phys. Rep. **520**, 253 (2012).
[66] C. Becker, S. Stellmer, P. Soltan-Panahi, S. Dörscher, M. Baumert, E.-M. Richter, J. Kronjäger, K. Bongs, and K. Sengstock, Nat. Phys. **4**, 496 (2008).
[67] M. Bruderer, A. Klein, S. R. Clark, and D. Jaksch, Phys. Rev. A **76**, 011605(R) (2007).
[68] M. Greiner, O. Mandel, T. Esslinger, T. W. Hänsch, and I. Bloch, Nature (London) **415**, 39 (2002).
[69] D. Jaksch and P. Zoller, Ann. Phys. (NY) **315**, 52 (2005).
[70] R. Gati, M. Albiez, J. Fölling, B. Hemmerling, and M. Oberthaler, Appl. Phys. B: Lasers Opt. **82**, 207 (2006).
[71] R. Gati and M. K. Oberthaler, J. Phys. B: At., Mol. Opt. Phys. **40**, R61 (2007).
[72] Y. Wu and V. S. Batista, J. Chem. Phys. **121**, 1676 (2004).
[73] P. A. J. Sherratt, D. V. Shalashilin, and M. S. Child, Chem. Phys. **322**, 127 (2006).
[74] S. Habershon, J. Chem. Phys. **136**, 054109 (2012).
[75] M. A. C. Saller and S. Habershon, J. Chem. Theory Comput. **13**, 3085 (2017).
[76] J. P. Alborzpour, D. P. Tew, and S. Habershon, J. Chem. Phys. **145**, 174112 (2016).
[77] T. Murakami and T. J. Frankcombe, J. Chem. Phys. **149**, 134113 (2018).
[78] J. A. Green, A. Grigolo, M. Ronto, and D. V. Shalashilin, J. Chem. Phys. **144**, 024111 (2016).
[79] J. A. Green and D. V. Shalashilin, Chem. Phys. Lett. **641**, 173 (2015).
[80] A. I. e. a. Streltsov, The Multiconfigurational Time-Dependent Hartree for Bosons Package, http://mctdhb.org.
[81] D. V. Shalashilin, M. S. Child, and D. C. Clary, J. Chem. Phys. **120**, 5608 (2004).
[82] K. Sakmann, A. I. Streltsov, O. E. Alon, and L. S. Cederbaum, Phys. Rev. A **89**, 023602 (2014).
[83] A. Grigolo, T. F. Viscondi, and M. A. M. de Aguiar, J. Chem. Phys. **144**, 094106 (2016).
[84] D. V. Shalashilin, J. Chem. Phys. **148**, 194109 (2018).
[85] O. E. Alon, A. I. Streltsov, and L. S. Cederbaum, J. Chem. Phys. **127**, 154103 (2007).
[86] L. Cao, V. Bolsinger, S. I. Mistakidis, G. M. Koutentakis, S. Krönke, J. M. Schurer, and P. Schmelcher, J. Chem. Phys. **147**, 044106 (2017).
[87] J. A. Green and D. V. Shalashilin, Data associated with "Simulation of the Quantum Dynamics of Indistinguishable Bosons with the Method of Coupled Coherent States", University of Leeds, https://doi.org/10.5518/595 (2019).
[88] M. Edwards, R. J. Dodd, C. W. Clark, and K. Burnett, J. Res. Natl. Inst. Stand. Technol. **101**, 553 (1996).